ARTICLE IN PRESS

Polyhedron xxx (2012) xxx–xxx

Contents lists available at SciVerse ScienceDirect

Polyhedron

journal homepage: www.elsevier.com/locate/poly

A series of mononuclear nickel(II) complexes of Schiff-base ligands having N,N,O- and N,N,N-donor sites: Syntheses, crystal structures, solid state thermal property and catecholase-like activity

Averi Guha [a], Kazi Sabnam Banu [a], Sudhanshu Das [a], Tanmay Chattopadhyay [b], Ria Sanyal [a], Ennio Zangrando [c,*], Debasis Das [a,*]

[a] *Department of Chemistry, University of Calcutta, 92, A.P.C. Road, Kolkata 700 009, India*
[b] *Department of Chemistry, Panchakot Mahavidyalya, Sarbari, Neturia, Purulia 723 121, India*
[c] *Dipartimento di Scienze Chimiche e Farmaceutiche, University of Trieste, Via L. Giorgieri 1, 34127 Trieste, Italy*

ARTICLE INFO

Article history:
Available online xxxx

Dedicated to Alfred Werner on the 100th Anniversary of his Nobel prize in Chemistry in 1913.

Keywords:
Mononuclear nickel(II) complex
X-ray crystallography
Thermogravimetry
Catecholase activity

ABSTRACT

Four new mononuclear nickel(II) complexes, namely $[NiL^1(H_2O)_3](NO_3)_2$ (**1**), $[NiL^2(H_2O)_3](NO_3)_2$ (**2**), $[NiL^3(H_2O)_3](NO_3)_2$ (**3**) and $[NiL^4(ClBz)(H_2O)]\cdot 1.25(H_2O)$ (**4**) have been synthesized via Schiff-base formation by condensation between 2-benzoylpyridine and *N*-(2-aminoethyl)pyrrolidine for L^1, salicylaldehyde and *N*-(2-aminoethyl)piperazine (L^2), 5-chlorosalicylaldehyde and *N*-(2-aminoethyl)piperazine (L^3), and 5-chlorosalicylaldehyde and *N*-(2-aminoethyl)morpholine (L^4). These complexes are comprehensively characterized via routine physicochemical techniques as well as by single crystal X-ray structural analyses. Despite all the nickel complexes are mononuclear, the catecholase activity shows prominent variation depending on the coordination environment around the metal center. Complexes **2** and **3** derived from same amine bear an extra positive charge on the ligand system facilitating the substrate–catalyst interaction to promote the oxidation of 3,5-DTBC to 3,5-DTBQ. On the contrary complexes **1** and **4** remain inert in nature, although **1** shows structural similarities in terms of coordination environment with nickel substituted catechol oxidase.

1. Introduction

For a long period of time considerable attention has been paid to the chemistry of the metal complexes of Schiff-bases containing nitrogen and other donors [1] and it has become an emerging area of research. Modern chemists still synthesize Schiff-bases that, if well-designed, are considered “privileged ligands”. The corresponding metal complexes have attracted increasing interest that may be attributed to their stability, biological activity [2] and potential applications in many fields such as in catalysis [3], material sciences, hydrometallurgy and also to get insight into molecular processes occurring in biochemistry [4–11]. Nickel(II) has very fascinating coordination chemistry owing to its inherent ability to adopt various geometries, which often interconvert and such configurational switch is generally associated with color changes. In recent years the development of nickel bio-chemistry and the use of nickel compounds in the construction of new magnetic materials give a thrust in this area. Our group is continuously engaged in studying Schiff-base complexes of transition and post-transition metal ions, mainly as small synthetic analogs of metallobiosites like catechol oxidase, phosphatase, cytP-450 and as possible mimics of nucleases [12]. Our work on modeling of catechol oxidase [13], (a type-III copper protein catalyzing exclusively the oxidation of catechols to quinones), demonstrates an extraordinary efficiency of metal complexes towards this reaction. In particular this activity takes place when extra positive charges either on imine nitrogen or other (usually nitrogen) atom are present on the ligand system. It has already been verified that mononuclear copper complexes are less active compared to their dinuclear counterparts. However, with manganese system the reverse trend is observed to be reality [12c,12e]. Till date rare reports were found in the literature where dinuclear or polynuclear nickel(II) complexes of Schiff-base ligands have been used as catalysts in the oxidation of catechols to quinones [12b,12f,12g]. Amongst these, one of our dinuclear nickel(II) complexes having a positively charged ligand system is observed to display a high activity [12b]. However, to the best of our knowledge no systematic study of mononuclear nickel(II) complexes of Schiff-base ligands is reported in the literature on this subject. For the present study we have designed four Schiff-base ligands L^1–L^4 (Scheme 1), and we are reporting herein the synthesis and the comprehensive characterization of four mononuclear nickel(II) complexes along with their spectroscopic, solid state thermal property and catecholase-like activity using

---

* Corresponding authors. Tel.: +91 33 24837031; fax: +91 33 23519755.
E-mail address: dasdebasis2001@yahoo.com (D. Das).

0277-5387/$ - see front matter © 2012 Elsevier Ltd. All rights reserved.
http://dx.doi.org/10.1016/j.poly.2012.07.088

Please cite this article in press as: A. Guha et al., Polyhedron (2012), http://dx.doi.org/10.1016/j.poly.2012.07.088

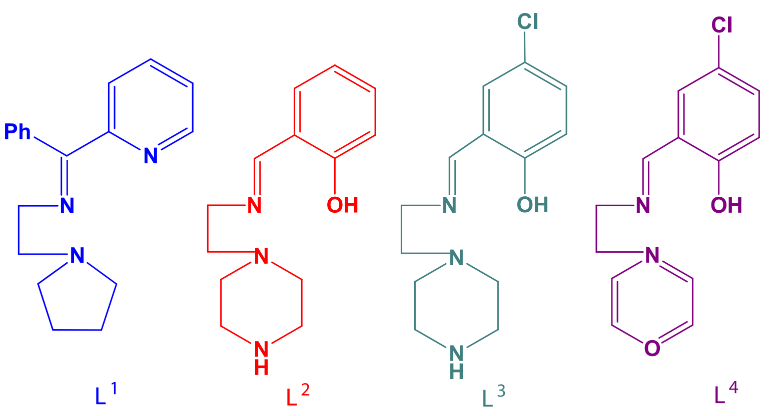

Scheme 1. Chemical drawing of the ligand systems.

3,5-di-*tert*-butylcatechol as model substrate. Of these, L^2 and L^3 should get protonated upon coordination in order to confirm our preliminary observations on the effect of this feature in the catalysis.

2. Experimental

2.1. Materials

All the chemicals salicylaldehyde, 5-chlorosalicylaldehyde, 2-benzoylpyridine, *N*-(2-aminoethyl)piperazine, *N*-(2-aminoethyl)pyrrolidine, *N*-(2-aminoethyl)morpholine and nickel nitrate hexahydrate were obtained from commercial sources and used as received. All other chemicals are of AR grade. Solvents were dried according to standard procedure and distilled prior to use.

2.2. Physical measurements

Elemental analyses (carbon, hydrogen and nitrogen) were performed using a Perkin Elmer 24 °C elemental analyzer. Infrared spectra were recorded on KBr disks (400–4000 cm^{-1}) with a Shimadzu FTIR-8400S. Electronic spectra (800–200 nm) were recorded at 27 °C using a Shimadzu UV-3101PC in dry methanol. Thermal analyses (TG–DTA) were carried out on a Mettler Toledo (TGA/SDTA 851) thermal analyzer in flowing nitrogen at a rate of 30 cm^3 min^{-1}. Ambient temperature magnetic susceptibility measurements were performed with Magway MSB Mk1 magnetic susceptibility balance. Cyclic voltammetry was performed using a BAS electrochemical workstation (Model Epsilon) under nitrogen atmosphere in conventional three electrode configurations with tetraethylammonium perchlorate as the supporting electrolyte in DMF. A planar platinum milli-electrode and a platinum wire were used in cyclic voltammetry as the working electrode and counter electrode, respectively. The potentials are reported with respect to Ag/AgCl as reference and are uncorrected for liquid junction potential.

2.3. Syntheses of the complexes

2.3.1. $[NiL^1(H_2O)_3](NO_3)_2$ (**1**)

A methanolic solution (5 mL) of *N*-(2-aminoethyl)pyrrolidine (0.2284 g, 2 mmol) was added dropwise to a hot methanolic solution (10 mL) of 2-benzoylpyridine (0.3664 g, 2 mmol) and the resulting solution was refluxed for 12 h till a light yellow color appeared. Then, a methanolic solution (10 mL) of $Ni(NO_3)_2{\cdot}6H_2O$ (0.727 g, 2.5 mmol) was added and the resulting solution was stirred for 3–4 h. The green solution was filtered, kept in a $CaCl_2$ desciccator in dark and after a few days crystals suitable for X-ray data analysis were obtained. (Yield 70%). *Anal.* Calc. for $C_{18}H_{27}N_5NiO_9$ (**1**): C, 41.88; H, 5.27; N, 13.57. Found: C, 41.85; H, 5.26; N, 13.55%. UV–Vis-NIR (in methanol, nm) λ_{max} = 590, 770, 895.

2.3.2. $[NiL^2(H_2O)_3](NO_3)_2$ (**2**)

A methanolic solution (5 mL) of *N*-(2-aminoethyl)pipeazine (0.258 g, 2 mmol) was added dropwise to a hot methanolic solution (10 mL) of salicylaldehyde (0.244 g, 2 mmol) and the resulting solution was refluxed for half an hour. Then, a methanolic solution (10 mL) of $Ni(NO_3)_2{\cdot}6H_2O$ (0.727 g, 2 mmol) was added stirring the resulting solution for 3–4 h. The green solution was filtered, kept in a $CaCl_2$ desiccator in dark and after a few days crystals suitable for X-ray data analysis were obtained. (Yield 73%). *Anal.* Calc. for $C_{13}H_{25}N_5NiO_{10}$ (**1**): C, 33.21; H, 5.36; N, 14.90. Found: C, 33.20; H, 5.33; N, 14.87%. UV–Vis-NIR (in methanol, nm) λ_{max} = 378, 614, 750, 900.

2.3.3. $[NiL^3(H_2O)_3](NO_3)_2$ (**3**)

A methanolic solution (5 mL) of *N*-(2-aminoethyl)piperazine (0.258 g, 2 mmol) was added dropwise to a hot methanolic solution (10 mL) of 5-chloro-salicylaldehyde (0.312 g, 2 mmol) and the resulting solution was refluxed for an hour. Then, a methanolic solution (10 mL) of $Ni(NO_3)_2{\cdot}6H_2O$ (0.727 g, 2 mmol) was added and the resulting solution was stirred for 3–4 h. The green solution was filtered, kept in a $CaCl_2$ desiccator in dark and after a few days crystals suitable for X-ray data analysis were obtained. (Yield 71%). *Anal.* Calc. for $C_{13}H_{24}ClN_5NiO_{10}$ (**1**): C, 30.95; H, 4.79; N, 13.88. Found: C, 30.92; H, 4.75; N, 13.86%. UV–Vis-NIR (in methanol, nm) λ_{max} = 387, 614, 754, 915.

2.3.4. $[NiL^4(ClBz)(H_2O)].1.25(H_2O)$ (**4**)

A methanolic solution (5 mL) of *N*-(2-aminoethyl)morpholine (0.2603 g, 2 mmol) was added dropwise to a hot methanolic solution (10 mL) of 5-chloro-salicylaldehyde (0.312 g, 2 mmol) and the resulting solution was refluxed for an hour. Then, a methanolic solution (10 mL) of $Ni(NO_3)_2{\cdot}6H_2O$ (0.727 g, 2 mmol) was added and the resulting solution was stirred for 3–4 h. The green solution was filtered and kept in a $CaCl_2$ desiccator in dark. Crystals suitable for X-ray data analysis were obtained after a few days. (Yield 68%). *Anal.* Calc. for $C_{20}H_{24.5}Cl_2N_2NiO_{6.25}$ (**1**): C, 45.97; H, 4.73; N, 5.36. Found: C, 45.95; H, 4.70; N, 5.33%. UV–Vis-NIR (in methanol, nm) λ_{max} = 385, 607, 755, 914.

Please cite this article in press as: A. Guha et al., Polyhedron (2012), http://dx.doi.org/10.1016/j.poly.2012.07.088

2.4. X-ray structure determination

Diffraction data for compounds **1–4** were collected on a Bruker Smart Apex diffractometer equipped with CCD. All the experiments were performed at room temperature (except for **1** carried out at 273 K) with Mo Kα radiation ($\lambda = 0.71073$ Å). Cell refinement, indexing and scaling of the data set were carried out using Bruker Smart Apex and Bruker Saint packages [14]. The structures were solved by direct methods and subsequent Fourier analyses and refined by the full-matrix least-squares method based on F^2 with all observed reflections [15]. The contribution of H atoms (at calculated position generated by program SHELXL [15] or located from the Fourier map for water molecules) was introduced in the final cycles of refinement. The ΔFourier map of **4** evidences an area of disordered electron density interpreted as three water oxygen atoms (one at half occupancy based on peak height). Crystallographic data and details of refinements are reported in Table 1. All the calculations were performed using the WinGX System, Ver 1.80.05 [16].

3. Results and discussion

3.1. Syntheses and characterization

All four complexes are prepared by applying template synthesis technique by treating a methanolic solution of nickel(II) nitrate hexahydrate with the Schiff-base formed in situ between aldehyde/ketone (salicylaldehyde, 5-chloro-salicylaldehyde and 2-benzoylpyridine) and amines [*N*-(2-aminoethyl)piperazine, *N*-(2-aminoethyl)pyrrolidine, *N*-(2-aminoethyl)morpholine]. Elemental analyses suggest that the molecular composition of the complexes should be $NiL^{1-3}(NO_3)_2\cdot 3H2O$ for complexes **1–3** and $NiL^4(NO_3)_2\cdot 2H_2O$ for complex **4**, which was further verified by thermogravimetric analyses. It is evident from the thermograms (please see SI) that all four complexes upon heating finally converted to NiO. For complex **1**, T_f (final temperature of decomposition) was 480 °C, to which the experimental weight loss corresponds to 86.83% (calculated 85.50%). The correspondent figures for **2** were $T_f = 430$ °C, exp. weight loss = 86.47% (calc. 84.10%); for **3**, $T_f = 590$ °C, exp. weight loss = 85.65% (calc. 87.01%) and for **4**, $T_f = 550$ °C, exp. weight loss = 85.60% (calc. 85.90%). The metal content in the final residual species in each case has been estimated by the usual gravimetric analysis [17] and the results corroborate well with the calculated metal content based on the compound formulation. Magnetic susceptibility measurements ($\mu_{eff} = \sim 3.2$ B.M.)

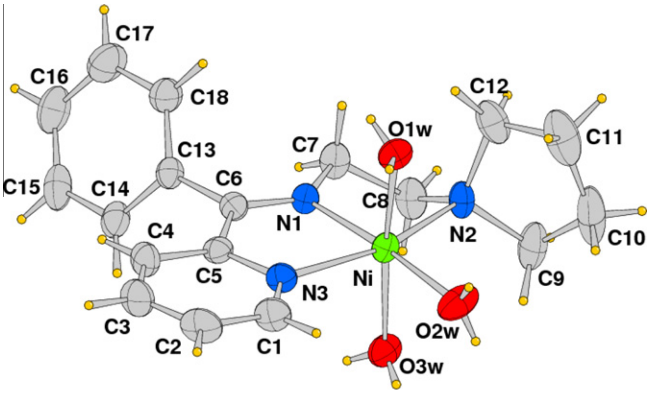

Fig. 1. ORTEP drawing (30% ellipsoid probability) and atom numbering scheme of the complex cation of **1**.

Table 2
Coordination bond lengths (Å) and angles (°) for **1**.

Ni–N(1)	2.004(3)	Ni–O(1w)	2.077(3)
Ni–N(2)	2.168(3)	Ni–O(2w)	2.034(3)
Ni–N(3)	2.110(3)	Ni–O(3w)	2.078(3)
N(1)–Ni–N(2)	81.71(13)	N(2)–Ni–O(3w)	88.39(15)
N(1)–Ni–N(3)	77.56(13)	N(3)–Ni–O(1w)	88.65(13)
N(1)–Ni–O(1w)	95.53(13)	N(3)–Ni–O(2w)	96.95(14)
N(1)–Ni–O(2w)	174.40(14)	N(3)–Ni–O(3w)	91.12(14)
N(1)–Ni–O(3w)	93.32(13)	O(1w)–Ni–O(2w)	85.34(12)
N(2)–Ni–N(3)	159.20(14)	O(1w)–Ni–O(3w)	170.88(13)
N(2)–Ni–O(1w)	95.05(14)	O(2w)–Ni–O(3w)	85.64(13)
N(2)–Ni–O(2w)	103.74(14)		

Table 1
Crystallographic data for compounds **1–4**.

	1	**2**	**3**	**4**.1.25H_2O
Empirical formula	$C_{18}H_{27}N_5NiO_9$	$C_{13}H_{25}N_5NiO_{10}$	$C_{13}H_{24}ClN_5NiO_{10}$	$C_{20}H_{24.5}Cl_2N_2NiO_{6.25}$
fw	516.16	470.09	504.53	522.53
Crystal system	orthorhombic	triclinic	triclinic	monoclinic
Space group	P bca	$P\bar{1}$	$P\bar{1}$	$P\,2_1/c$
a (Å)	11.9136(18)	9.337(2)	9.035(5)	18.049(4)
b (Å)	17.157(3)	9.829(3)	9.804(5)	13.117(3)
c (Å)	23.278(3)	12.672(3)	13.264(7)	20.279(5)
α (°)		94.981(4)	71.918(6)	
β (°)		100.287(4)	79.389(6)	99.419(3)
γ (°)		118.349(4)	64.748(6)	
V (Å)	4758.2(12)	987.1(4)	1008.4(10)	4736.2(18)
Z	8	2	2	8
D_{calc}, g cm^{-3}	1.441	1.582	1.662	1.466
μ (Mo Kα), mm^{-1}	0.872	1.045	1.157	1.083
F(000)	2160	492	524	2164
θ range (°)	1.75–28.34	2.40–28.30	2.38–26.28	1.86–26.58
No. of reflections collected	26745	8145	6855	33373
No. of independent reflections	5625	4359	3547	9097
R_{int}	0.0691	0.0204	0.0408	0.0345
No. of reflections [$I > 2\sigma(I)$]	3487	3728	2608	6735
No. of refined parameters	310	262	289	580
Goodness-of-fit (F^2)	1.113	0.999	1.012	1.042
R_1, wR_2 ($I > 2\sigma(I)$)[a]	0.0788,0.1509	0.0437, 0.1289	0.0699, 0.2038	0.0651, 0.2082
Residuals (e Å^3)	0.880, −0.344	0.564, −0.348	1.571, −1.487	1.647, −0.452

[a] $R_1 = \Sigma||F_o| - |F_c||/\Sigma|F_o|$, $wR_2 = [\Sigma w(F_o^2 - F_c^2)^2/\Sigma w(F_o^2)^2]^{1/2}$.

reveal that nickel(II) attains an octahedral configuration in all the complexes and the appearance of three bands in UV–Vis–NIR region corroborate this coordination geometry [18]. All the complexes exhibit IR bands due to C═N stretch in the range 1638–1648 cm^{-1} and skeletal vibration in the range 1549–1560 cm^{-1}. Broad bands centered in the range 1360–1385 cm^{-1} are exhibited by the complexes **1**–**3** due to the presence of nitrate ion. The very strong and broad bands observed at ~3383, ~3370, ~ 3407, and ~3361 cm^{-1} in **1**–**4**, respectively, are attributed to hydrogen bonded O–H stretches of water molecules present in the complexes. In order to understand the composition in solution, molar conductance of the 10^{-3} M methanol solution of complexes **1**–**4** were determined. The conductance values at 298 K for **1**–**4** are 175, 185, 180 and 7 Ω^{-1} cm^2 M^{-1}, respectively, indicating that **1**–**3** behave as 2:1 electrolytes, while complex **4** is non-electrolytic in nature.

3.2. Description of crystal structure

The ORTEP view of the complex cation of **1**, $[NiL^1(H_2O)_3](NO_3)_2$, with the atom numbering scheme is illustrated in Fig. 1 and a selection of bond distances and angles is reported in Table 2. The independent unit contains two nitrate anions beside the metal complex. The nickel ion shows a severely distorted octahedral geometry where three co-ordination sites are occupied by N donor atoms from the pyridine, the imino and the pyrrolidine, with

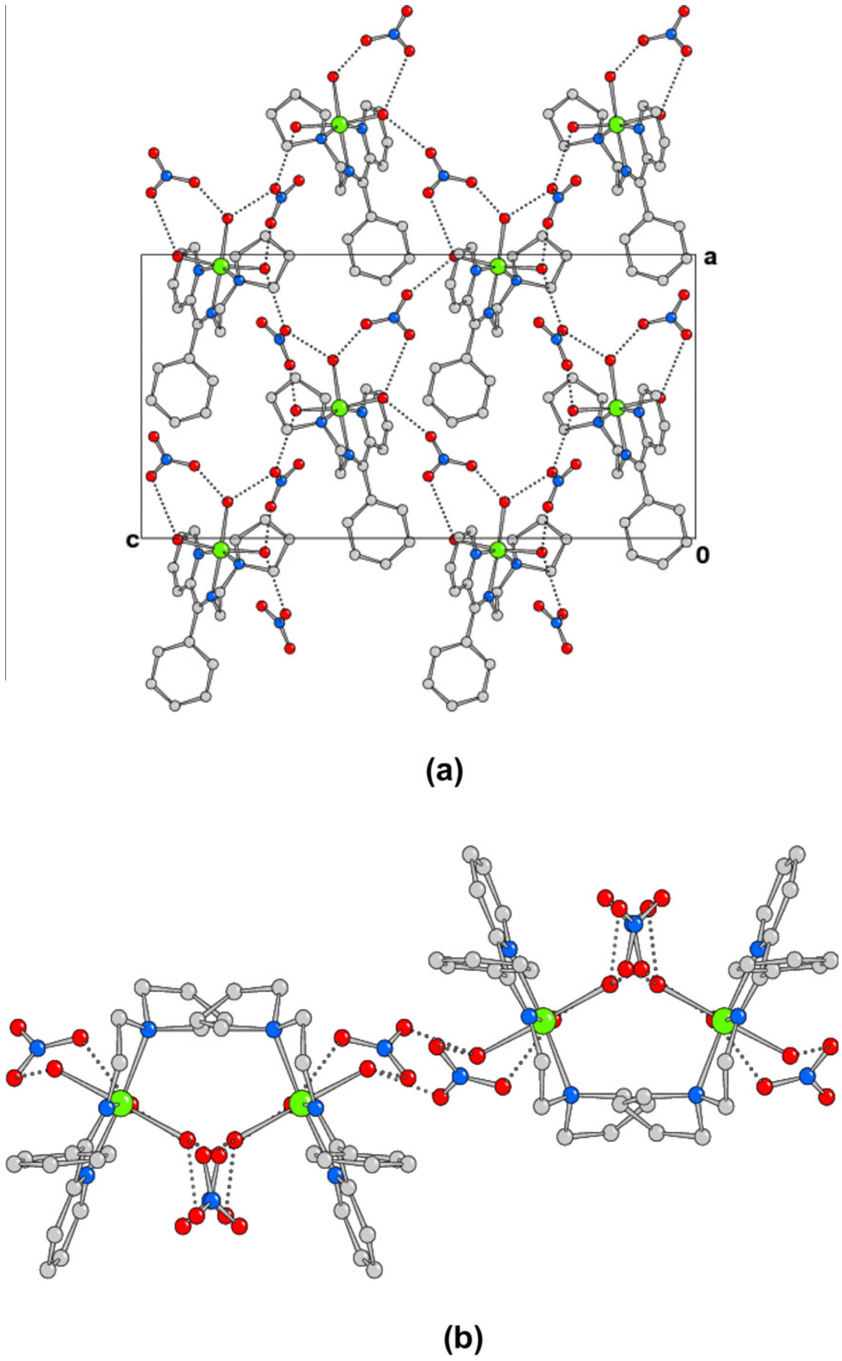

Fig. 2. (a) View along axis *b* of the 2D network in compound 1 formed by H-bonds realized among the aqua ligands and nitrate anions. (b) Side view of the 2D layer down axis *a*.

Please cite this article in press as: A. Guha et al., Polyhedron (2012), http://dx.doi.org/10.1016/j.poly.2012.07.088

Table 5
Hydrogen bond parameters in complexes **1**–**4**.

D–H	d(D–H)	d(H…A)	<DHA	d(D…A)	A	Symmetry code of A
Complex **1**						
O1w–H12	0.760	2.014	170.36	2.766	O1	
O1w–H11	0.844	1.933	173.15	2.773	O3	[x−1/2, y, −z+1/2]
O2w–H21	0.776	1.942	168.52	2.707	O4	
O2w–H22	0.704	2.001	178.13	2.705	O1	[x−1/2, y, −z+1/2]
O3w–H31	0.803	1.897	167.64	2.687	O5	[x+1/2, −y+1/2, −z+1]
O3w–H32	0.702	2.200	178.89	2.902	O6	
Complex **2**						
N3–H3b	0.901	2.224	145.25	3.009	O5	[x, y+1, z]
N3–H3b	0.901	2.052	152.30	2.880	O7	[x, y+1, z]
N3–H3a	0.901	2.028	153.22	2.861	O9	[−x+1, −y+1, −z]
N3–H3a	0.901	2.302	144.35	3.079	O10	[−x+1, −y+1, −z]
O1w–H2c	1.022	2.039	157.80	3.010	O7	
O1w–H2d	0.754	2.510	123.35	2.992	O10	
O2w–H4c	0.792	1.849	169.25	2.631	O1	[−x, −y, −z]
O2w–H4d	0.960	1.911	162.19	2.840	O9	[x−1, y, z]
O3w–H3c	0.812	2.060	161.70	2.842	O5	[x−1, y, z]
O3w–H3d	0.990	1.763	166.25	2.734	O8	[x−1, y, z]
Complex **3**						
N3–H3a	0.900	2.388	144.56	3.164	O5	[x, y−1, z]
N3–H3a	0.900	1.976	155.46	2.820	O7	[x, y−1, z]
N3–H3b	0.900	2.151	142.14	2.914	O9	[−x+1, −y+1, −z+1]
N3–H3b	0.900	2.200	150.79	3.018	O10	[−x+1, −y+1, −z+1]
O1w–H11	0.846	2.217	170.40	3.055	O7	[x−1, y, z]
O1w–H12	0.844	2.289	129.86	2.903	O8	[x−1, y, z]
O2w–H21	0.847	1.992	157.65	2.794	O9	
O2w–H22	0.931	1.693	174.40	2.621	O1	[−x, −y+2, −z+1]
O3w–H31	0.860	2.061	178.34	2.921	O5	
O3w–H32	0.844	1.897	168.68	2.730	O8	
Complex **4**						
O1w–H11w	0.850	1.930	172.59	2.775	O6	
O2w–H21w	0.864	2.010	137.53	2.710	O2	
O1w–H12w	0.828	2.111	168.26	2.927	O3w[a]	
O2w–H22w	0.871	2.000	142.80	2.745	O4w[a]	

[a] O3w and O4w are lattice water molecules of which no H atom was positioned.

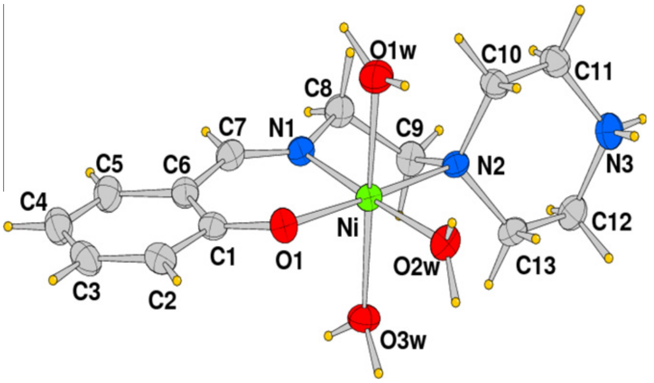

Fig. 3. ORTEP drawing of the complex cation of **2**.

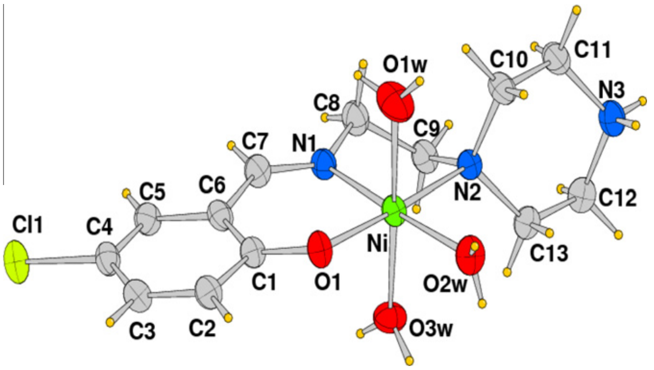

Fig. 4. ORTEP drawing of the complex cation of **3**.

formation of two 5-membered chelate rings. The metal completes the coordination environment with three water molecules (Fig. 1).

Among the Ni–N bond distances, that involving the imino N donor is the shorter (2.004(3) Å), while the Ni–N(py) is of 2.110(3) Å, and the Ni–N(pyrrolidine) is the longest for the sp^3 hybridization of the nitrogen atom (2.168(3) Å). Correspondingly the Ni–O2w bond length, trans to the imino nitrogen, is significantly shorter (2.034(3) Å) with regard to the other Ni–Ow values of 2.077(3) and 2.078(3) Å. The distortion can be further evidenced from the deviation of the cisoid and transoid angles from the ideal values (Table 2).

The nitrate anions behave as H-bond acceptor towards the aqua ligands resulting in the formation of a 2D undulated layered network, and a view of the packing down axis-b is shown in Fig. 2, while the geometrical parameters of H-bonds are collected in Table 5. The compounds **2** and **3** crystallize in same space group (triclinic system, $P\bar{1}$) and are isostructural, being the unit cell parameters close comparable, differing by ca. 20 Å^3 in their volume, being larger in **3** for the presence of the chlorine atom. A thermal ellipsoid diagram of **2** and **3** along with the atom numbering scheme is given Figs. 3 and 4, respectively. In both the complexes the metal ions have a distorted octahedral environment with the coordination sites occupied by the tridentate Schiff base through the phenoxo oxygen, the imino nitrogen and the N donor of the piperazine moiety and by three water molecules. The structural similarity that appears from the figures of the two complexes is also confirmed by the Ni–N and Ni–O coordination distances reported in Table 3

Please cite this article in press as: A. Guha et al., Polyhedron (2012), http://dx.doi.org/10.1016/j.poly.2012.07.088

Table 3
Coordination bond lengths (Å) and angles (°) for **2** and **3**.

	Complex **2**		Complex **3**
Ni–N(1)	1.994(2)	Ni–N(1)	1.995(5)
Ni–N(2)	2.241(2)	Ni–N(2)	2.216(5)
Ni–O(1)	2.003(2)	Ni–O(1)	1.988(4)
Ni–O(1w)	2.122(2)	Ni–O(1w)	2.127(5)
Ni–O(2w)	2.025(2)	Ni–O(2w)	2.023(4)
Ni–O(3w)	2.113(2)	Ni–O(3w)	2.110(4)
N(1)–Ni–N(2)	82.76(9)	N(1)–Ni–N(2)	83.48(17)
N(1)–Ni–O(1)	91.47(9)	N(1)–Ni–O(1)	91.63(17)
N(1)–Ni–O(1w)	90.66(10)	N(1)–Ni–O(1w)	89.2(2)
N(1)–Ni–O(2w)	175.00(9)	N(1)–Ni–O(2w)	176.26(17)
N(1)–Ni–O(3w)	90.42(9)	N(1)–Ni–O(3w)	89.18(18)
N(2)–Ni–O(1)	174.04(8)	N(2)–Ni–O(1)	175.05(15)
N(2)–Ni–O(1w)	92.32(9)	N(2)–Ni–O(1w)	91.91(19)
N(2)–Ni–O(2w)	92.24(9)	N(2)–Ni–O(2w)	92.79(17)
N(2–)–Ni–O(3w)	87.32(9)	N(2)–Ni–O(3w)	88.44(17)
O(1)–Ni–O(1w)	89.21(10)	O(1)–Ni–O(1w)	88.75(19)
O(1)–Ni–O(2w)	93.52(9)	O(1)–Ni–O(2w)	92.10(17)
O(1)–Ni–O(3w)	91.26(9)	O(1)–Ni–O(3w)	90.76(18)
O(1w)–Ni–O(2w)	89.85(10)	O(1w)–Ni–O(2w)	91.0(2)
O(1w)–Ni–O(3w)	178.81(9)	O(1w)–Ni–O(3w)	178.31(19)
O(2w)–Ni–O(3w)	89.03(9)	O(2w)–Ni–O(3w)	90.67(19)

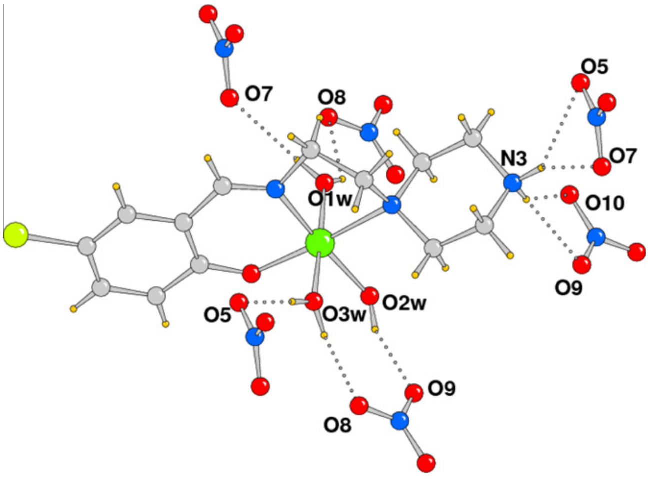

Fig. 5. H-bonding scheme in compound **3**. A similar arrangement is also observed in compound **2**.

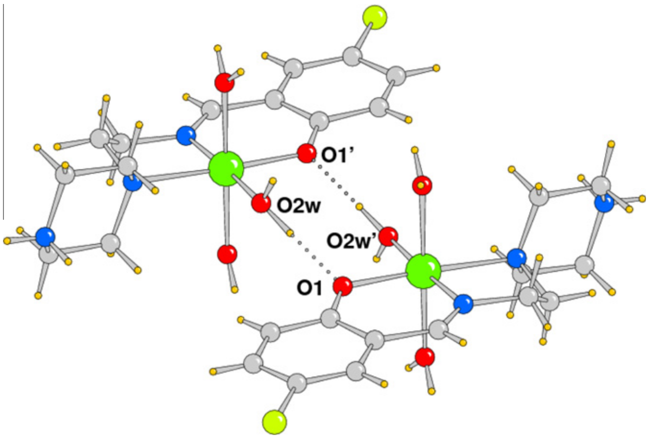

Fig. 6. The centrosymmetric pairing of complexes in **3** engaged in a double H-bond. A similar arrangement is also detected in compound **2**.

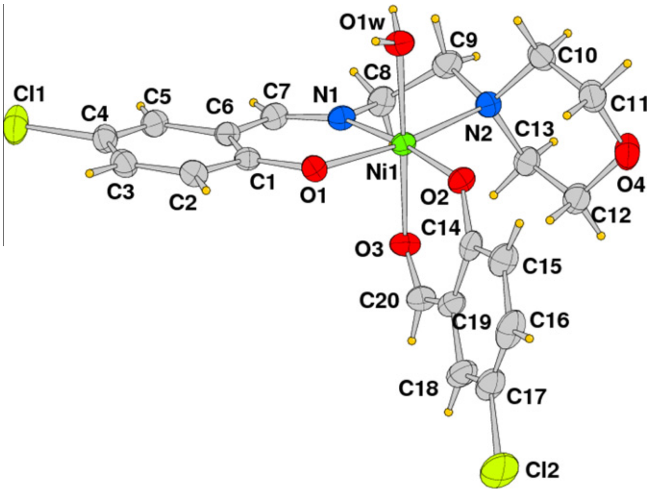

Fig. 7. ORTEP drawing (30% probability ellipsoid) of the molecular complex A of **4**.

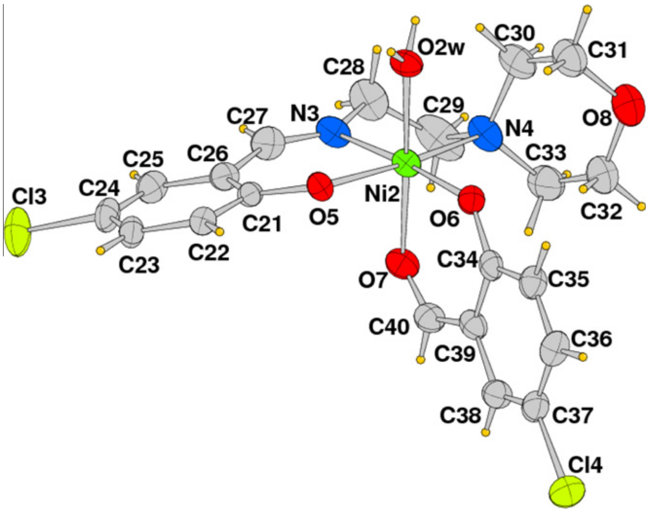

Fig. 8. ORTEP drawing (30% probability ellipsoid) of the molecular complex B of **4**.

Table 4
Coordination bond lengths (Å) and angles (°) for the two complexes of **4**.

Complex A		Complex B	
Ni(1)–N(1)	2.006(3)	Ni(2)–N(3)	2.018(4)
Ni(1)–N(2)	2.242(3)	Ni(2)–N(4)	2.224(4)
Ni(1)–O(1)	2.082(3)	Ni(2)–O(5)	2.101(3)
Ni(1)–O(2)	2.008(3)	Ni(2)–O(6)	1.992(3)
Ni(1)–O(3)	2.072(3)	Ni(2)–O(7)	2.061(3)
Ni(1)–O(1w)	2.094(3)	Ni(2)–O(2w)	2.084(3)
N(1)–Ni(1)–N(2)	82.53(13)	N(3)–Ni(2)–N(4)	84.22(17)
N(1)–Ni(1)–O(1)	89.62(12)	N(3)–Ni(2)–O(5)	87.22(15)
N(1)–Ni(1)–O(2)	173.89(13)	N(3)–Ni(2)–O(6)	174.82(15)
N(1)–Ni(1)–O(3)	86.16(12)	N(3)–Ni(2)–O(7)	88.28(15)
N(1)–Ni(1)–O(1w)	94.06(13)	N(3)–Ni(2)–O(2w)	92.11(15)
N(2)–Ni(1)–O(1)	170.90(12)	N(4)–Ni(2)–O(5)	171.44(14)
N(2)–Ni(1)–O(2)	100.57(12)	N(4)–Ni(2)–O(6)	100.27(15)
N(2)–Ni(1)–O(3)	93.38(12)	N(4)–Ni(2)–O(7)	88.23(15)
N(2)–Ni(1)–O(1w)	88.40(12)	N(4)–Ni(2)–O(2w)	94.79(15)
O(1)–Ni(1)–O(2)	87.68(11)	O(5)–Ni(2)–O(6)	88.27(12)
O(1)–Ni(1)–O(3)	90.68(12)	O(5)–Ni(2)–O(7)	91.30(12)
O(1)–Ni(1)–O(1w)	87.57(11)	O(5)–Ni(2)–O(2w)	85.72(12)
O(2)–Ni(1)–O(3)	88.39(11)	O(6)–Ni(2)–O(7)	89.27(13)
O(2)–Ni(1)–O(1w)	91.31(12)	O(6)–Ni(2)–O(2w)	90.10(13)
O(3)–Ni(1)–O(1w)	178.23(12)	O(7)–Ni(2)–O(2w)	176.97(13)

Please cite this article in press as: A. Guha et al., Polyhedron (2012), http://dx.doi.org/10.1016/j.poly.2012.07.088

where the corresponding values are well comparable. In fact for each Ni center, the bond length involving the imine nitrogen is the shortest (1.994(2) and 1.995(5) Å in **2** and **3**, respectively) and comparable in length with the metal-phenoxo of 2.003(2) 1.988(4) Å. On the other hand the Ni–N(piperidine) is the longest (2.241(2), 2.216(5) Å). The Ni–O(water) bond distances show intermediate values and lie in the range 2.023(4)–2.127(5) Å. Thus the presence of the chorine atom in the tridentate ligand of **3** does not seem to affect the coordination distances with respect to **2**.

The piperazine ring assume the expected chair conformation and the presence of two nitrate anions in each compound indicates the protonation of piperazine nitrogen atom N3, as confirmed by the bifurcated H-bonds formed by the NH_2^+ group with nitrate anions. The H-bonding scheme is comparable in the two structures leading to a 3D network. A detail of the H-bond interactions involving the water molecules, the amino group N3 and nitrate anion is shown in Fig. 5 for complex **3**. Moreover the complexes are paired in the crystal about a center of symmetry giving rise to a double H-bond (Fig. 6) for compound **3** (O2w…O1′ = 2.621 Å, O2w–H…O1′ = 174.40°). The corresponding figures in **2** are 2.631 Å, 169.25°. The ligand L^2, as well as the correspondent having a nitro group in para position of the phenolato ring, has already been reported in similar triaquo Ni(II) derivatives having sulfate as counterion [19]. In those complexes the reported Ni–O and Ni–N distances follow a trend close comparable to those of **2** and **3**, as expected for high spin Ni(II) complexes reported so far.

The X-ray structural analysis of compound **4** evidenced two independent neutral complexes, depicted in Figs. 7 and 8, respectively, beside disordered lattice water molecules. In both the complexes (hereinafter indicated A and B) the nickel ion adopts a distorted octahedral geometry being chelated by the tridentate Schiff base meridionally bound through the phenolic oxygen, the imino nitrogen and the N donor of the morpholine moiety, and in addition by an unreacted 5-chloro-salicylaldehyde anion, completing the coordination geometry by an aqua ligand. The Ni–N and N–O bond lengths and angles are comparable in the two complexes within their esd's (Table 4). The Ni–N(imine) bond distances are significantly shorter than the Ni–N(morpholine) ones, as expected for the different hybridization of the N atoms, but also to accomplish the five-membered Ni(NH_2–CH_2–CH_2–NH_2) ring. The Ni1–O2 and Ni2–O6 bond distances of the salicylaldehyde phenoxo oxygen, of 2.009(3) and 1.992(3) Å, are shorter with respect the other Ni–O ones, which range from 2.061(3) to 2.101(3) Å. The coordination bond distances of the tridentate ligand agree with those measured in **2** and **3** with the exception of the Ni–O(phenoxo) that are sensibly longer here (mean 2.09 versus 2.00 Å).

A distinguished feature is the different conformation (δ and λ) assumed by the ethylenediamine (en) in the two independent complexes A and B (see Fig. 9). Incidentally, due to the centrosymmetric space group the correspondent enantiomer of each is present in the unit cell. The Fig. 9 evidences also the slight different arrangement of the ligands about the metal ion, may be due to packing requirements or induced by the interactions occurring in the crystal between A and B (see below). In particular the iminophenolato moiety in A is almost coplanar with the equatorial plane N1/N2/O1/O2 (dihedral angle of 6.6(1)°), while the correspondent figure in B (with plane N3/N4/O5/O6) is of 15.5(5)°.

The two molecules A and B are firmly connected by two H-bonds occurring between the aquo ligand and the hydroxy-benzaldehyde anion of the other complex (O1w…O6 = 2.775(4), O2w…O2 = 2.710(4) Å) and through π–π interactions between phenolato rings C1 and C14 of molecule A with aromatic rings C34 and C21 of B (centroid to centroid distance of 3.539(3) and 3.571(3) Å, respectively). The pair of complexes along with the interactions between them are shown in Fig. 10. As mentioned in the experimental part, the electron density map evidences an area filled by solvent molecules, rather difficult to model and interpreted as two lattice water molecules plus another at half occupancy based on the peak height. These molecules, O3w, O4w and O5w, are H-bond connected with the aqua ligands and also among them, connecting two A–B pair of complexes.

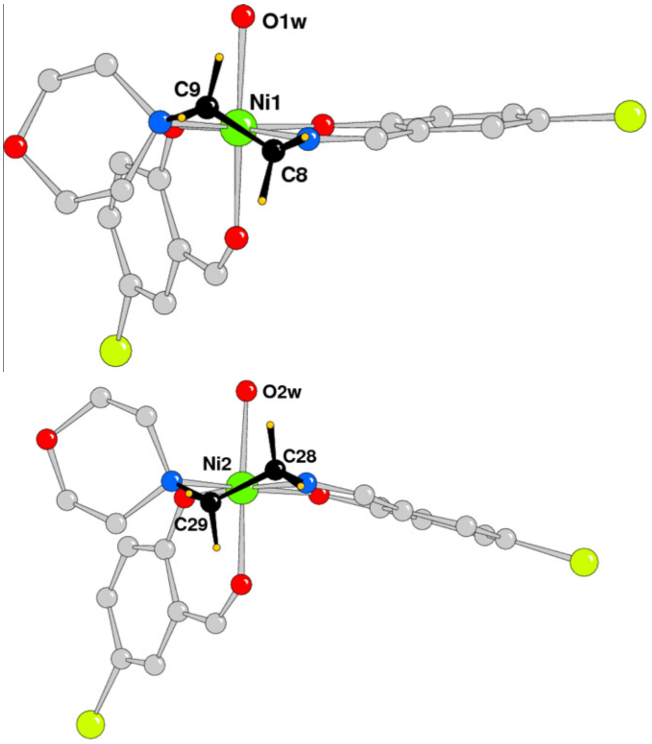

Fig. 9. Perspective view of the two conformational isomers of the five-membered Ni(NH_2–CH_2–CH_2–NH_2) ring in molecule A and B.

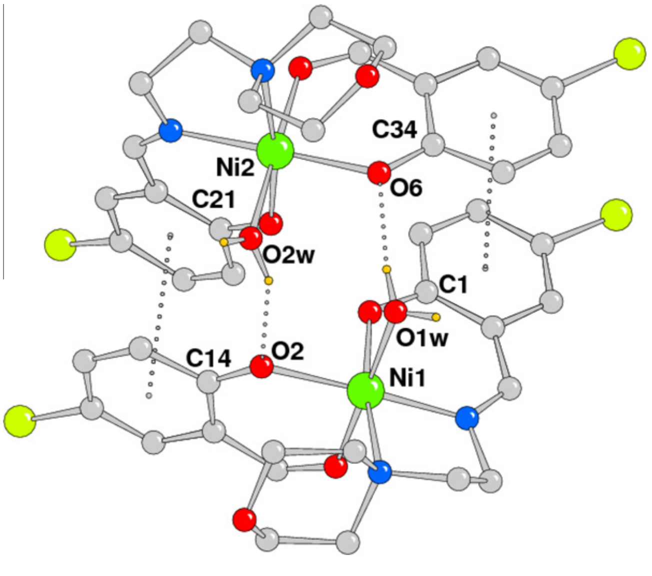

Fig. 10. H-bonds and π–π aromatic ring interactions occurring between the two independent complexes of **4**.

The ligand L^4, but lacking of the chlorine atom, was used in the construction of an unprecedented tetranuclear cyclic Ni cluster where the metals are bridged by EE azide anions [20]. The Ni–N and N–O distances involving the tridentate ligand and the water molecule of the four metal centers compare well with those here reported.

Please cite this article in press as: A. Guha et al., Polyhedron (2012), http://dx.doi.org/10.1016/j.poly.2012.07.088

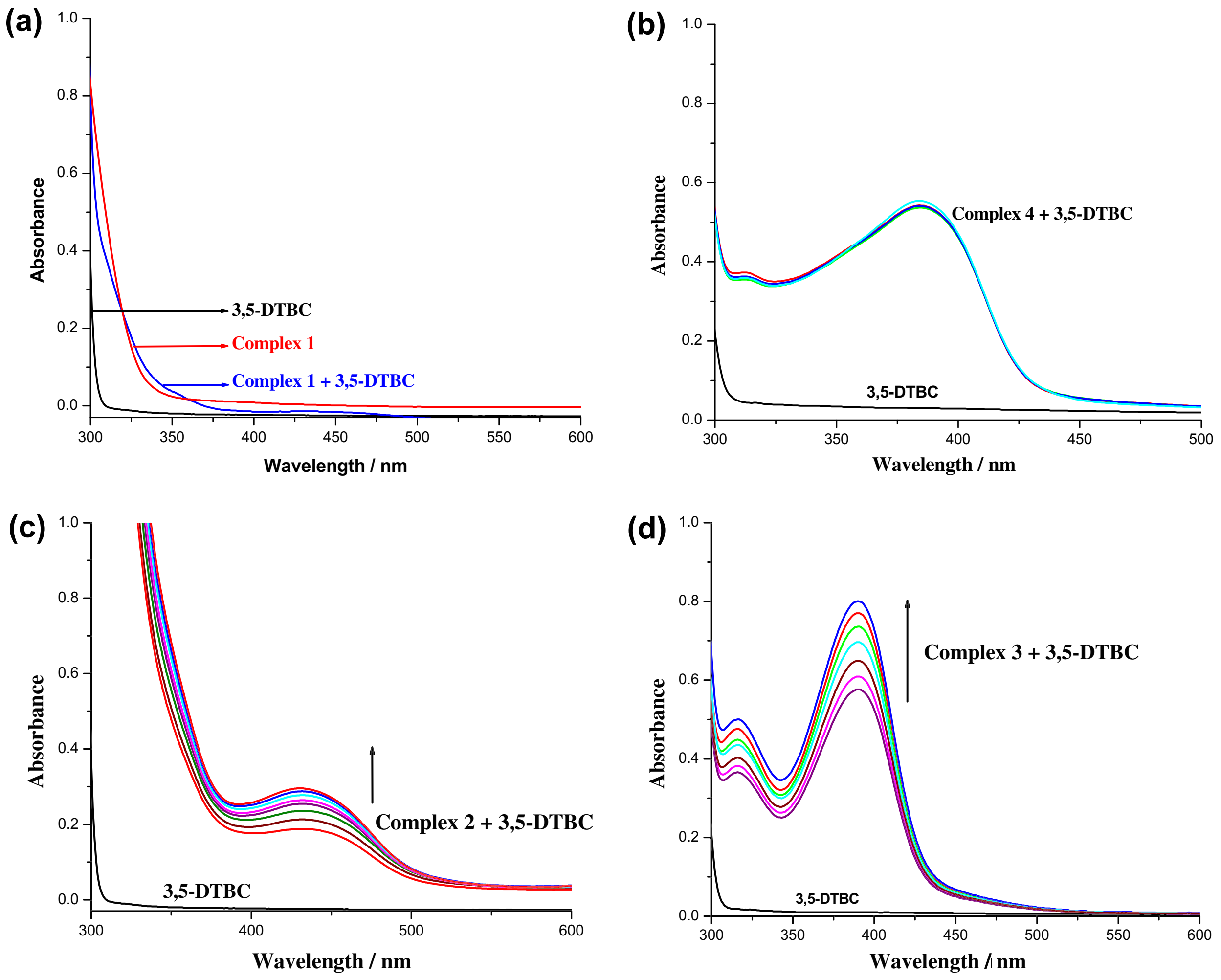

Fig. 11. The changes of UV–Vis spectral behavior at regular interval of time for (a) complex **1**, (b) complex **4**, (c) complex **2**, (d) complex **3** in methanol medium upon addition of 3,5-DTBC.

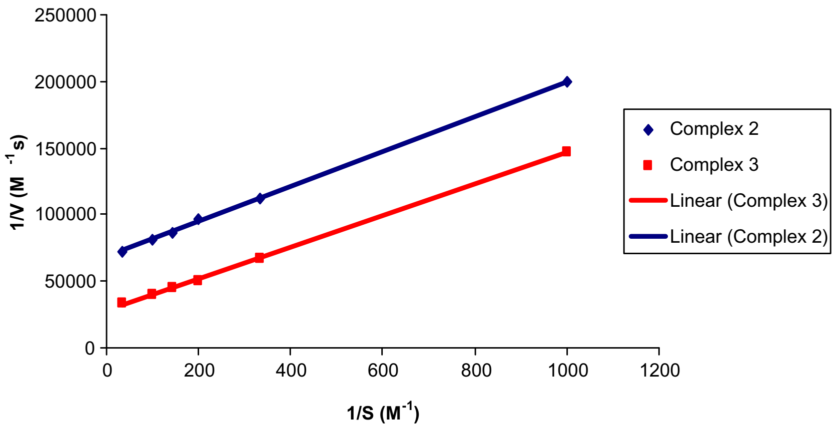

Fig. 12. Lineweaver–Burk plots of complexes **2** and **3**.

Table 6
Kinetic parameters for catecholase-like activity of **2** and **3** in MeOH medium.

Complex	Wavelength (nm)	V_{max} (Ms^{-1})	K_M (M)	k_{cat} (h^{-1})
2	430	1.46×10^{-5}	1.92×10^{-3}	5.26×10^{1}
3	395	3.57×10^{-5}	4.24×10^{-5}	1.29×10^{2}

3.3. Catechol oxidase activity

In order to study the catecholase-like activity of present mononuclear nickel(II) complexes, 3,5-di-*tert*-butylcatechol (3,5-DTBC) has been chosen as the substrate. This molecule with two bulky t-butyl substituents on the ring has a low quinone–catechol

Please cite this article in press as: A. Guha et al., Polyhedron (2012), http://dx.doi.org/10.1016/j.poly.2012.07.088

reduction potential. This makes it easily oxidized to the corresponding o-quinone, 3,5-di-*tert*-butylbenzoquinone (3,5-DTBQ), which is highly stable and shows a maximum absorption at about 400 nm in methanol. To check the ability of the Ni(II) complexes to act as catalysts for catecholase-like activity, a 1×10^{-4} mol dm^{-3} solution of a complex is treated with 1×10^{-2} mol dm^{-3} (100 equiv) of 3,5-DTBC under aerobic condition. The course of the reaction was followed by UV–Vis spectroscopy, and the time dependent spectral scans of the four complexes are depicted in Fig. 11. From the figure it is evident that a band ~390 nm is observed to increase with time after addition of 3,5-DTBC due to the gradual increment of concentration of 3,5-DTBQ in case of complexes **2** and **3** catalyzed reactions, whereas nearly no change is noticed in the spectral pattern of complexes **1** and **4**. This data unambiguously demonstrate that **2** and **3** are active catalysts for the aerial oxidation of 3,5-DTBC to 3,5-DTBQ, whereas **1** and **4** reveal to be inactive. The crystal structure analyses of **2** and **3** pointed out that a positive charge center is created on the piperazine nitrogen atom, as we previously observed in dinuclear Cu(II) and Ni(II) complexes with 2,6-bis(N-ethylpiperazine-iminomethyl)-4-methyl-phenol as ligand. This observation gives once again support to our earlier suggestion [12b] that the positively charged piperazine moiety, present in the tridentate ligand of complexes **2** and **3**, creates a channel to facilitate the catalyst–substrate interaction, a prerequisite for exhibiting better catalytic activity. A similar proposal has now well accepted, especially to explain the activity of the Cu/Zn-superoxide dismutase (SOD), where the Cu(II) lies at the bottom of a narrow channel, and the positively charged arginine and lysine residues are supposed to play a role in attracting the anions guiding them through the channel towards the active site [21–23]. Here it is noteworthy that in enzymes, the protein super-structure provides inherent spatial constraints that channels can be formed that limit substrate access to the metal center within a buried active site. It is difficult to imagine that similar scenarios can be operating for our mononuclear complexes in which there is limited steric protection on along the z-axis of the nickel centers. However, it may be assumed that the extra positive charge on the backbone of the ligand system is of immense help to facilitate the substrate-metal center interaction via electrostatic as well as H-bonding interaction. The conversion of catechol to quinone is a two-electron oxidation process, and most of the investigators working with copper catechol oxidase model systems believe that the metal center redox participation is responsible for the catechol to quinone conversion [24]. The electrochemical analyses of complexes **2** and **3** in methanol are featureless, suggesting no preference for the nickel(II) ions to undergo reduction to nickel(I) or oxidation to nickel(III). However, when the same experiment is done in presence of 3,5-DTBC we observed reduction peaks at +0.28 and −1.10 V which may be attributed to reduction of 3,5-DTBQ and that of Ni(II) to Ni(I), respectively and only one oxidation peak at +1.15 V corresponds to the oxidation of 3,5-DTBC to the quinone. Thus, it may be stated that in presence of 3,5-DTBC our nickel(II) complexes undergo reduction with concomitant oxidation of the catechol to quinone. Therefore it may be assumed that the metal center redox participation is responsible for the catecholase-like activity of the complexes. It is to note that in spite of our several attempts we failed to find out the oxidation peak corresponds to the oxidation of Ni(I) to Ni(II).

The kinetics for the oxidation of the substrate 3,5-DTBC were determined by the initial rates method at 25 °C. The concentration of the substrate 3,5-DTBC was always kept at least 10 times larger than that of the complex and the increase of respective quinone concentration were determined at a particular wavelength for each complex. Solutions of substrates of concentration ranging from 0.001 to 0.05 mol dm^{-3} were prepared from a concentrated stock solution in methanol. 2 mL of the substrate solution were poured in a 1 cm spectrophotometer quartz cell thermostated at 25 °C. Then 0.04 mL of 0.005 mol dm^{-3} complex solution was quickly added to it so that the ultimate concentration of the complex becomes 1×10^{-4} mol dm^{-3}. The dependence of the initial rate on the concentration of substrate, spectrophotometrically monitored at respective wavelength, is given as SI file. Moreover the initial rates method shows a first-order dependence on complex concentration and exhibited saturation kinetics at higher substrate concentrations. For this reason, a treatment based on Michaelis–Menten model was seemed to be appropriate. The values of Michaelis binding constant (K_m), maximum velocity (V_{max}) and rate constant for the dissociation of substrates (i.e., turnover number, k_{cat}) were calculated for each complex from the Lineweaver–Burk graph of 1/V versus 1/[S] (Fig. 12) by using the equation $1/V = \{K_m/V_{max}\}\{1/[S]\} + 1/V_{max}$. The enzyme kinetics data are listed in Table 6. From this study it is evident that, although mononuclear nickel(II) complexes with appropriate Schiff-base ligands are exhibiting catecholase-like activity with 3,5-DTBC as model substrate, their efficiency is lower in comparison to the analogous dinuclear nickel(II) species for which a $k_{cat} = 1.44 \times 10^4$ h^{-1} was derived [12b].

4. Conclusion

Four mononuclear nickel(II) complexes with designed Schiff-base ligands have been synthesized and comprehensively structurally characterized with the aim to investigate their catecholase-like activity. Crystal structure analysis revealed that complex **1** exhibits coordination environment around metal center very much similar as in the native catechol oxidase in met state, but it is inactive in catalyzing the oxidation of catechol. Complex **4**, containing an unreacted phenolate ligand, appears not to have further affinity to interact with catechol substrate. On the other hand, complexes **2** and **3** are highly active in catalyzing the oxidation of 3,5-DTBC to 3,5-DTBQ, and the positive charged ligand system of these is supposed to be instrumental for their catecholase-like activity.

Acknowledgement

The authors wish to thank the CSIR for Research Project, [01(2464)/11/EMR-II dt 16-05-11 to DD] and Shailabala Biswas Research Foundation, University of Calcutta (AG) for financial support.

Appendix A. Supplementary data

CCDC 878600–878603 contains the supplementary crystallographic data for complexes **1** to **4**. These data can be obtained free of charge via http://www.ccdc.cam.ac.uk/conts/retrieving.html, or from the Cambridge Crystallographic Data Centre, 12 Union Road, Cambridge CB2 1EZ, UK; fax: (+44) 1223-336-033; or e-mail: deposit@ccdc.cam.ac.uk. Supplementary data associated with this article can be found, in the online version, at http://dx.doi.org/10.1016/j.poly.2012.07.088.

References

[1] (a) P. Bhattacharya, J. Parr, A.T. Ross, J. Chem. Soc. Dalton (1998) 3149;
(b) S.S. Djebbar, B.O. Benali, J.P. Deloume, Polyhedron 16 (1997) 2175.
[2] C.M. Liu, R.G. Xiong, X.Z. You, Y.J. Liu, K.K. Cheung, Polyhedron 15 (1996) 4565.
[3] S.S. Djebbar, B.O. Benali, J.P. Deloume, Transition Met. Chem. 23 (1998) 443.
[4] N.F. Curtis, Coord. Chem. Rev. 3 (1968) 273.
[5] V. Alexander, Chem. Rev. 95 (1995) 273.
[6] H. Okawa, H. Furutachi, D.E. Fenton, Coord. Chem. Rev. 174 (1998) 51.
[7] L.F. Lindoy, The Chemistry of Macrocyclic Ligand Complexes, Cambridge University, Cambridge, UK, 1989.
[8] P. Guerriero, S. Tamburini, P.A. Vigato, Coord. Chem. Rev. 139 (1995) 17.

[9] O. Khan, in: A.G. Sykes (Ed.), Advances in Inorganic Chemistry, Academic Press, S. Diego, USA, 1995, p. 179.

[10] K.S. Murray, in: A.G. Sikes (Ed.), Advances in Inorganic Chemistry, vol. 43, Academic Press, S. Diego, USA, 1995, p. 261.

[11] A. Martell, J. Penitka, D. Kong, Coord. Chem. Rev. 216 (2001) 55.

[12] (a) K.S. Banu, T. Chattopadhyay, A. Banerjee, S. Bhattacharaya, E. Suresh, M. Nethaji, E. Zangrando, D. Das, Inorg. Chem. 47 (2008) 7083;
(b) T. Chattopadhyay, M. Mukherjee, A. Mondal, P. Maiti, A. Banerjee, K.S. Banu, S. Bhattacharya, B. Roy, D.J. Chattopadhyay, T.K. Mondal, M. Nethaji, E. Zangrando, D. Das, Inorg. Chem. 49 (2010) 3121;
(c) K.S. Banu, T. Chattopadhyay, A. Banerjee, M. Mukherjee, S. Bhattacharya, G.K. Patra, E. Zangrando, D. Das, Dalton Trans. (2009) 8755;
(d) K.S. Banu, T. Chattopadhyay, A. Banerjee, S. Bhattacharya, E. Zangrando, D. Das, J. Mol. Catal. A: Chem. 310 (2009) 34;
(e) A. Guha, K.S. Banu, A. Banerjee, T. Ghosh, S. Bhattacharya, E. Zangrando, D. Das, J. Mol. Catal. A: Chem. 338 (2011) 51;
(f) A. Guha, A. Banerjee, R. Mondol, E. Zangrando, D. Das, J. Coord. Chem. 22 (2011);
(g) A. Banerjee, A. Guha, P. Maiti, S. Goswami, T. Chattopadhyay, T.K. Mondal, S. Bhattacharya, E. Zangrando, D. Das, Transition Met. Chem. (2011) 1.

[13] C. Gerdemann, C. Eicken, B. Krebs, Acc. Chem. Res. 35 (2002) 183.

[14] Bruker. *SMART*, *SAINT*. Software Reference Manual Bruker AXS Inc. Madison, Wisconsin, USA, 2000.

[15] G.M. Sheldrick, Acta Crystallogr., Sect. A 64 (2008) 112.

[16] L.J. Farrugia, J. Appl. Crystallogr. 32 (1999) 837.

[17] Vogel's Textbook of Quantitative Chemical Analysis, fifth ed., Pearson Education, Asia, 1989, pp. 336.

[18] A.B.P. Lever, Inorganic Electronic Spectroscopy, second ed., Elsevier Science Publishers B.V, Amsterdam, 1984. pp. 553.

[19] S. Mukhopadhyay, D. Mandal, D. Ghosh, I. Goldberg, M. Chaudhury, Inorg. Chem. 42 (2003) 8439.

[20] S. Sasmal, S. Hazra, P. Kundu, S. Majumder, N. Aliaga-Alcalde, E. Ruiz, S. Mohanta, Inorg. Chem. 49 (2010) 9517.

[21] J.A. Tainer, E.D. Getzoff, J.S. Richardson, D.C. Richardson, Nature 306 (1983) 284.

[22] J.S. Valentine, M.W. Pantoliano, Protein–metal ion interaction in Cupro-zinc Protein (Superoxide dismutase) (R), in: T.G. Spiro (Ed.), Copper Proteins, Krieger Publishing Co., Malabar, FL, 1981, p. 291.

[23] J.S. Valentine, D.J. Mota de Freitas, Chem. Educ. 62 (1985) 990.

[24] C. Eicken, B. Krebs, J.C. Sacchettini, Curr. Opin. Struct. Biol. 9 (1999) 677.

Please cite this article in press as: A. Guha et al., Polyhedron (2012), http://dx.doi.org/10.1016/j.poly.2012.07.088